Mathematical Medicine and Biology: A Journal of the IMA (2024) **41**, 382–403
https://doi.org/10.1093/imammb/dqae020
Advance Access publication on 18 October 2024

Polymer-interface-tissue model to estimate leachable release from medical devices

Martin L. Tanaka*
College of Engineering and Technology, Western Carolina University, Cullowhee, NC 28723, USA
*Corresponding author. Email: mtanaka@wcu.edu

David M. Saylor
Division of Biology, Chemistry, and Materials Science (DBCMS), Office of Science and Engineering Laboratories (OSEL), Center for Devices and Radiological Health (CDRH), US Food and Drug Administration, Silver Spring, MD 20993, USA

and

Robert M. Elder
Division of Biology, Chemistry, and Materials Science (DBCMS), Office of Science and Engineering Laboratories (OSEL), Center for Devices and Radiological Health (CDRH), US Food and Drug Administration, Silver Spring, MD 20993, USA

[Received on 11 December 2023; revised on 14 October 2024; accepted on 14 October 2024]

Abstract

The ability to predict clinically relevant exposure to potentially hazardous compounds that can leach from polymeric components can help reduce testing needed to evaluate the biocompatibility of medical devices. In this manuscript, we compare two physics-based exposure models: 1) a simple, one-component model that assumes the only barrier to leaching is the migration of the compound through the polymer matrix and 2) a more clinically relevant, two-component model that also considers partitioning across the polymer–tissue interface and migration in the tissue away from the interface. Using data from the literature, the variation of the model parameters with key material properties were established, enabling the models to be applied to a wide range of combinations of leachable compound, polymer matrix and tissue type. Exposure predictions based on the models suggest that the models are indistinguishable over much of the range of clinically relevant scenarios. However, for systems with low partitioning and/or slow tissue diffusion, the two-component model predicted up to three orders of magnitude less mass release over the same time period. Thus, despite the added complexity, in some scenarios it can be beneficial to use the two-component model to provide more clinically relevant estimates of exposure to leachable substances from implanted devices.

Keywords: biotransport; tissue diffusion; leachables; regulatory science; computational modelling; partition coefficient; migration; FDA; medical device.

1. Introduction

Implanted polymeric medical devices can pose a risk to human health when they contain potentially hazardous materials that leach into the body. Historically, extraction experiments and animal studies

have been used to estimate the amount of material released. Extraction studies conducted by companies seeking Food and Drug Administration (FDA) clearance or approval for new medical devices are product specific and conducted under harsh, non-physiological conditions (Turner *et al.*, 2020). While these studies are useful in the assessment of toxicological risk, the highly conservative assumptions provide little information to develop a generalizable understanding of the true clinical exposure to leachables released from polymeric devices. However, these approaches are changing. Fueled by increases in computational capabilities, computer models can now be used to predict the amount of material released over time. These simulations can complement traditional extraction studies and yield several benefits for regulatory science. First, the models can be used to simulate a more realistic environment than the harsh conditions used in extraction studies. Second, because the models contain system-specific input parameters, they can be easily adapted to other polymer types or leachable chemicals making it easy to analyse a multitude of different systems. Third, once the models are developed and validated, simulations can often be run in seconds saving the weeks or months needed for extraction studies. This may help medical device companies to accelerate new product development enabling new devices to reach the market faster, reduce animal use, decrease the effort needed to meet regulatory requirements and reduce overall product development costs.

Some of the first mathematical models developed to characterize leaching of potentially hazardous substances released from polymeric materials were conducted in conjunction with the Environmental Protection Agency (Schwope *et al.*, 1992). Leachable substances, including additives, catalyst residue, unreacted monomers, oligomers, plasticizers, etc., can have detrimental effects when released into the environment. The FDA is also concerned with leachable materials, which may be released into food from its packaging (Gandek, 1986) or from medical devices in contact with biological tissue (Saylor *et al.*, 2019; Saylor *et al.*, 2020).

Using data from extractables and leachables testing, mathematical models can be generated to estimate exposure based on the total amount of leachable substance contained within the implant. This approach requires assumptions to be made regarding the release rate of the leachable substance from the device under the clinical conditions of use. For a device that is in contact with the body for a long time such as an implanted medical device, one could assume an average daily release by dividing the total amount of leachable substance by the total time the device is in contact with the body (Saylor *et al.*, 2020). However, for most combinations of leachable substances and polymers, the initial release rate will be highest upon implantation and decrease over time. Thus, this simple, average rate model could underestimate the actual daily exposure during the initial period following implantation. A more conservative approach is to assume that the total amount of leachable substance contained within the device is released on the first day (FDA, 2023). While this model is more protective than the first, it can lead to exceedingly conservative and non-physical exposure estimates over longer timeframes.

To address this, physics-based models have been developed that include the properties that influence the release rate from a polymeric material in contact with the body (Saylor *et al.*, 2019; Saylor *et al.*, 2020). Movement of leachable substances contained within a polymeric implant may be modelled as solid-state diffusion. When a concentration gradient exists within the polymer, net migration will occur following the concentration gradient according to Fick's law (Crank, 1975),

$$\frac{\partial C\,(x,t)}{\partial t} = D_p \nabla^2 C\,(x,t) \tag{1}$$

where the concentration of the leachable substance, C, is a function of the position within the polymer, x, and time, t. D_p is the effective (macroscopic) diffusion coefficient of the leachable in the polymer. D_p

is scalar and independent of C, x and t. Using physics-based models, the FDA has developed regulatory science tools for rapid risk assessments of additives in medical devices. These tools predict the amount of material that may be released from an implanted polymeric medical device based on the model input parameters entered.

In this research, models will be extended beyond a one-component system (implant only) to a two-component system that includes the surrounding tissue. The mathematical models account for diffusion of leachables through a polymeric material, migration across the polymer–tissue interface and diffusion through the surrounding tissue. Physics-based models that better capture the complexities of this system may yield more clinically relevant results and expand our understanding of these complex biodynamic systems.

1.1. *Mathematical models*

1.1.1. *Two-component model.* A two-component mathematical model was developed to characterize the migration of leachable substances from an implanted polymeric device, across the polymer–tissue interface and through the surrounding tissue. The initial condition assumes that the leachable chemical is homogeneously distributed throughout the implant and no leachable substance is in the tissue prior to implantation. It also assumes that the polymeric implant will remain structurally intact throughout the duration of the simulation. If the polymer were to degrade or swell (e.g. a hydrogel), this would change the diffusion coefficient of the leachable within the polymer and would violate the model assumption of constant diffusivity. Human tissue surrounding the implant is modelled as a homogeneous material and assumed to be quasistatic with consistent material properties over the duration of the simulation. Although human tissue undergoes a multitude of histological and morphological changes in response to an implanted medical device and may include the formation of a fibrous capsule, these changes take time to develop, and our model assumes these to be minimal during the first 24 hours following implantation. Implants are modelled as a flat plate with a thickness of 2 L. Diffusion is one dimensional through the thickness and diffusion through the edges is considered negligible. Tissue is on both sides of the implanted device, so a symmetry boundary condition exists at the midplane.

The polymer-interface-tissue model is based on migration equations in Gandek's PhD thesis (Gandek, 1986), who studied the leaching of potentially hazardous materials from packaging into food. He developed a modelling tree to characterize different migration conditions including fluids with boundary layers, solids dominated by diffusive transport and well-mixed conditions. To model an implanted medical device surrounded by tissue, the scenario was selected, which modelled a finite polymer (the implant), infinite food (the tissue), and the case where movement of leachables in both are controlled by diffusion. The finite polymer represents a polymeric implant with a finite quantity of leachable contained within the device. The infinite tissue represents the relatively large mass of the human body and its ability to remove leached substances from the peri-implant tissue over time.

Important model parameters include D_p, the diffusivity of a leachable substance in the polymer, $K_{p:t}$, the polymer–tissue partition coefficient and D_t, the diffusivity of a leachable substance in the tissue. The polymer–tissue partition coefficient is the ratio of the solubility of a leachable substance in the polymer to its solubility in the tissue. Values of $K_{p:t} \neq 1$ cause a discontinuity in leachable concentration across the interface. To simplify and generalize the solution, dimensionless parameters were established. The first dimensionless parameter, $\mathrm{n}\tau$, is a time parameter that is scaled by the diffusion coefficient, D_p, and half the implant thickness, L.

$$\tau = \frac{D_p t}{L^2} \tag{2}$$

The dimensionless parameter associated with migration across the polymer–tissue interface and the relative migration rate within the polymer and tissue is:

$$\beta = \frac{1}{K_{p:t}}\sqrt{\frac{D_t}{D_p}} \tag{3}$$

The amount of material released, $M(\tau, \beta)$, is given by,

$$\frac{M(\tau,\beta)}{M_0} = \left(\frac{\beta}{1+\beta}\right) 2\sqrt{\tau}\left(\frac{1}{\sqrt{\pi}} - \left(\frac{\beta}{1+\beta}\right) 2\sum_{n=1}^{\infty}\left[\left(\frac{1-\beta}{1+\beta}\right)^{n-1} ierfc\left(\frac{n}{\sqrt{\tau}}\right)\right]\right) \tag{4}$$

This equation (Gandek, 1986) is an infinite series that converges on the analytical solution with an infinite number of terms. The number of terms necessary for convergence depends on the values of the input parameters.

1.1.2. *One-component model.* A one-component model was also considered for comparison. This model included only the implanted polymeric device and assumed a sink boundary condition at the polymer–tissue interface. A sink boundary condition yields a maximum release rate because it assumes that all leachable substances that reach the implant surface are instantly removed. Thus, there is no resistance to migration at the polymer surface. Like the two-component model, the initial condition assumes a homogeneous distribution of leachable substances within the polymeric implant and no degradation or swelling of the polymer over the duration of the analysis.

Solutions for non-steady state diffusion in a plane sheet with a uniform initial distribution and a fixed surface concentration were published by Crank (Crank, 1975). Two analytical solutions were provided, one for short evolution times (Crank Equation 4.20),

$$\frac{M(\tau)}{M_0} = 2\sqrt{\tau}\left(\frac{1}{\sqrt{\pi}} + 2\sum_{n=1}^{\infty}\left[(-1)^n ierfc\left(\frac{n}{\sqrt{\tau}}\right)\right]\right) \tag{5}$$

and one for long evolution times (Crank Equation 4.18),

$$\frac{M(\tau)}{M_0} = 1 - \sum_{n=0}^{\infty}\frac{8}{(2n+1)^2\pi^2}\exp\left(-\frac{\tau(2n+1)^2\pi^2}{4}\right) \tag{6}$$

Equation (5) requires fewer terms to converge when the dimensionless time parameter, τ, is small. Equation (6) has the opposite property. It requires fewer terms to converge when the dimensionless time parameter τ is large. By transitioning from equation (5) to equation (6) at $\tau = 0.2$, sufficiently accurate results can be achieved using only one term.

By substituting τ into equations (5) and (6) and taking only the first terms, an approximate solution for the Crank equations was obtained,

$$\frac{M(\tau)}{M_0} = \begin{cases} 2\sqrt{\frac{\tau}{\pi}} & \tau \le 0.2 \\ 1 - \frac{8}{\pi^2}\exp\left(-\frac{\tau\,\pi^2}{4}\right) & \tau > 0.2 \end{cases} \tag{7}$$

Notice that equation 7 is only dependent upon the dimensionless time parameter, τ, while equation 4 has both, τ and β. Because β accounts for differences in the solubility and diffusivity between the polymer and the tissue, it is not present in the one-component model that only considers diffusion through the polymer. Moreover, the one-component model and the two-component model are equivalent in the limit as $\beta \to \infty$ (see Supplemental Information—Mathematical Proof, 2.3).

1.1.3. *Numerical solution methods.* Computational models to calculate the amount of mass released were developed using MATLAB (R2021a, The MathWorks Inc., Natick, MA) based on equations (2–4, 7). The method is generally applicable and can be used to analyse a broad range of specific cases. Two cases are analysed to illustrate the method.

For the first case, bisphenol A (BPA) in silicone was selected due to its high polymer diffusion coefficient. BPA is a relatively small molecule that contributes to its high mobility and the silicone matrix has relatively low migration resistance. For all calculations, the first 70 terms of the infinite series were used to solve equation (4). This number of terms was determined to be sufficient for all input parameter values within the analysis range (see Supplemental Information—Model Convergence, SI2). Mass release was plotted as a function of time for the two-component model to observe model behaviour over an evolution time of 1 day and 30 days. Results for the one- and two-component models were plotted on the same graph for comparison.

For the second case, Irganox 1010 in high-density polyethylene (HDPE) was selected due to its low polymer diffusion coefficient. Irganox 1010 is a relatively large molecule that contributes to its low mobility and HDPE is semi-crystalline with a relatively high migration resistance. Mass release was calculated using the one- and two-component models and plotted over an evolution time of 1 day and 30 days. From the findings of Gandek, it was expected that minimal differences would be observed when β was greater than 10 and that resistance to migration would occur for smaller values of β leading to lower mass release predictions using the two-component model.

The time required to release 99% of the total mass was also calculated using MATLAB. Using the same equations (2–4, 7), the evolution time was extended until 99% of the initial mass of leachable substance within the device had enough time to be released. Mass release was plotted as a function of release time for both the one- and two-component models.

MATLAB code was also developed to estimate the mass release over the input parameter range to compare the differences obtained using the one- and two-component models. First, mass release using the two-component model was calculated and plotted as a colour-coded heat map over the input parameter range for β and τ. Next, results for the one-component model were calculated and plotted as a function of τ. The one-component model does not include β as a model parameter, so the results were plotted as a log–log line plot.

There may be conditions where the results found using the simpler one-component model are negligibly different than those found using the more complex two-component model. In order to determine when this situation may occur, the result found using the one-component model (Crank) was divided by the results for the same input parameter values using the two-component model (Gandek). This relationship was defined as the Crank to Gandek ratio (CGR). The CGR was calculated and plotted over the input parameter range for β and τ.

1.2. *Model input parameters*

Because the goal of the study is to provide a framework for a wide range of applications, a critical part of this research is to approximate values for each of the important model parameters over a sufficiently

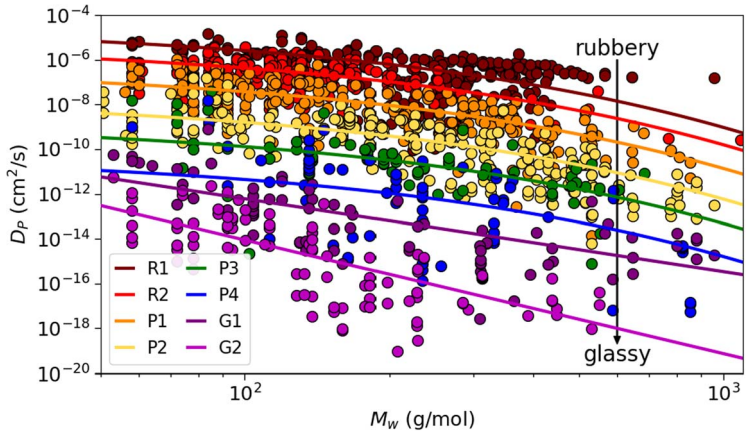

Figure 1 Diffusion coefficient of leachable substances in polymers at 37°C. Each colour represents a category of polymer chemistries with similar experimental diffusion coefficients. Rubbery polymers (e.g. PDMS, EPDM) have high diffusion coefficients, while glassy polymers (e.g. PEEK, PET) have low diffusion coefficients. The solid lines show the median DP values for polymers in each category estimated using empirical functional forms (Elder & Saylor, 2023)

large range. While model parameter data exist in published literature, it is not sufficiently organized or processed to be applied directly in the mathematical models. In this section, methods used to obtain data D_p, $K_{p:t}$ and D_t are presented.

1.2.1. *Estimating diffusion coefficients within a polymer.* The rate that a leachable substance diffuses through a polymer, D_p, is an important model input parameter for both the one-component and the two-component models. The value of D_p depends upon the characteristics of the leachable substance and the polymer matrix in which it is diffusing. Thus, a different value of D_p exists for each leachable—polymer pairing. With thousands of leachable substances and dozens of commonly used implantable polymers, the number of combinations is large. Experimental data exist for many of these combinations, but there are many more that have not been experimentally measured. To address this lack of data, structure–property relationships have been developed that used characteristics of the leachable substance (e.g. molecular weight) and the characteristics of the polymer (e.g. crystallinity and glass transition temperature) to predict values of D_p for combinations where experimental data do not exist (Saylor *et al.*, 2019; Saylor *et al.*, 2020). Recent efforts have produced data sets that characterize the diffusion coefficient for over 1000 chemical–polymer combinations (Elder & Saylor, 2023).

D_p can be estimated using empirical functional forms (Elder & Saylor, 2023). In prior work, we determined appropriate functional forms for a variety of polymers grouped into categories with similar experimental diffusion coefficients. These categories are termed rubbers (R1–2), plastics (P1–4) and glasses (G1–2). In our prior work, we used these functional forms and continuous probability distributions to define upper bounds on D_p. In this work, we instead use quantiles (e.g. the median or 50th quantile) to estimate D_p (Fig. 1). For the rubbers and plastics categories, we use the so-called Piringer model (Piringer & Baner, 2008), which is an empirical relation between D (cm^2/s), M_w (g/mol) and T (K):

$$D_{pir}\left(M_w, T\right) = 10^4 \exp\left[A_P - 0.1351 M_w^{\frac{2}{3}} + 0.003 M_w - \frac{E_A}{RT}\right] \tag{8}$$

Table 1 *Median parameter values (M_w >50 g/mol)*

Category	Representative polymers	Median parameters
R1	Silicone	$A_P = 14.25$
R2	EPDM, natural rubber	$A_P = 12.46$
P1	LDPE, polyurethane	$A_P = 10.02$
P2	Polypropylene, Teflon	$A_P = 6.87$
P3	HDPE, poly(vinyl acetate)	$A_P = 4.36$
P4	Nylon, poly(lactic acid)	$A_P = 0.97$
G1	Polystyrene, PEEK	$\alpha = -13.18$, $\beta = -3.25$
G2	PET, PMMA	$\alpha = -8.95$, $\beta = -5.08$

Table 2 *D_p quantiles*

Quantile	5%	25%	Median	75%	95%
Value	1.9×10^{-15}	3.4×10^{-10}	3.2×10^{-8}	4.9×10^{-7}	1.2×10^{-5}

where D_{pir} is the diffusion coefficient of the leachable in the polymer, M_w is the molecular weight of the leachable, $E_A/R = 10{,}454$ K is an activation energy normalized by the gas constant R and A_P is a category-specific empirical parameter. For the glasses categories, we use a different functional form, a power law:

$$\ln D_{pow}\left(M_w\right) = \alpha + \beta \ \ln M_w \tag{9}$$

where α and β are empirical category-specific parameters. The parameters that define the median value for each category (A_P for rubbers and plastics, α and β for glasses) are given in Table 1, which also includes a partial list of polymers included in each category. Note that these parameters only apply for M_w >50 g/mol, and different parameters are needed for M_w ≤50 g/mol. Additional methodological details and parameters for lower and upper bounds are presented in the Supplemental Information (Leachable Diffusivity in Polymers, SI1).

The data in Fig. 1 were analysed to determine the median diffusion coefficient for all polymers in the dataset, the upper and lower quartiles and the 5% and 95% values (Table 2). Examination of these data shows that using an input parameter range for D_p from 1.9×10^{-15} to 1.2×10^{-5} cm^2/s captures a large portion of polymer–leachable combinations.

1.2.2. *Estimating migration across the interface.* To determine the biotransport behaviour across the polymer–tissue interface, the partition coefficient is needed. The polymer–tissue partition coefficient, $K_{p:t}$, is a measure of the ratio of the concentration of a leachable within the polymer to the concentration of a leachable within the tissue in equilibrium. Often a dominating factor influencing this parameter is the hydrophilicity/hydrophobicity of a leachable substance. Hydrophobic substances tend to stay within the polymer avoiding the polar water molecules present in most tissue. This can result in a discontinuity in leachable concentration at the interface that may be modelled as a step function. Hydrophilic substances being leached from an implanted device will readily leave the typically hydrophobic polymer and pass across the interface into the tissue. Values of $K_{p:t} \neq 1$ will result in a step function change in concentration of the leachable across the boundary. Note that the two-component model assumes a solid polymer to solid tissue interface. For scenarios where the device is in contact with a static (well-mixed)

liquid phase, more appropriate models can be adopted (Gandek, 1986). Alternatively, the two-component model can be used with Dt > > Dp as a good approximation. If there is substantive advective flow removing the leachable from the peri-implant environment, e.g. blood flow, the one component model that assumes a sink boundary condition at the interface would provide a reasonable approximation.

$K_{p:t}$ can be found by comparing the solubility of a leachable in a polymer, S_p, to the solubility of a leachable in a tissue S_t, where

$$K_{p:t} = \frac{S_p}{S_t} \tag{10}$$

Thus, values for $K_{p:t}$ can be determined if values for S_p and S_t can be obtained. Note that S_p depends upon the specific type of leachable substance and the type of polymer in which it is dissolved. Similarly, S_t depends upon the type of leachable substance and the type of tissue in which it is dissolved. As a result, $K_{p:t}$ is a function of all three materials, the type of leachable substance, the polymer type and the tissue type.

To specify $K_{p:t}$, we start by recognizing that $S_p = K_{p:w} \times S_w$, where $K_{p:w}$ is the polymer–water partition coefficient and S_w is the solute's water solubility. Data for $K_{p:w}$and S_w were used to obtain values for S_p. A polymer/solute solubility database was generated by conducting a literature search for solubility measurements in any polymer, at any temperature, for any solute, and using any experimental method. The database contains about 7600 data points for over 100 polymers, over 800 solutes and nearly 2700 polymer/solute systems. Solubility data were also obtained from the commercially available Dortmund Data Bank (Dortmund, 2023), which added about 4400 points, 50 polymers, 200 solutes and 1500 systems. The solubility of a solute in a polymer is reported in various forms, most commonly the polymer–water partition coefficient, the infinite dilution activity coefficient ($\Omega^{\infty} = 1/S_p$) or the Henry's law constant ($H = S_p/P_{sat}$, where P_{sat} is the saturation vapour pressure) (Suné, 2006). Less commonly, the solubility is reported directly as S_p, e.g. via sorption experiments (Mańin *et al.*, 1998; Chandrasekar *et al.*, 2018) or by creating binary polymer/solute mixtures with increasing solute concentrations (Haddadin *et al.*, 2009). Solubility data in any of these forms were collected and appropriate data were used to convert them to S_p and $K_{p:w}$. A literature review was conducted to find values for S_t. A systematic search using SciFinder (ACS, 2022), Medline/PubMed (NIH, 2022b) and Google Scholar (Google, 2023) was conducted using several keywords and phrases. While the solubility of leachable substances in tissue was not readily available in the literature, information about plasma-tissue partition coefficients was published and used to calculate tissue solubility. Utsey *et al.* (2020) discussed five mathematical models based on mechanistic equations, the Poulin and Theil method (Poulin & Theil, 2000; Poulin *et al.*, 2001; Poulin & Theil, 2002), the Berezhkovskiy method (Berezhkovskiy, 2004), the Rogers and Rowland method (Rodgers *et al.*, 2005; Rodgers & Rowland, 2006), the Schmitt *et al.* method (Schmitt, 2008), and the PK-Sim standard method (Willmann *et al.*, 2005; Lippert *et al.*, 2019). While all of these models have merit for specific applications, overall, none were shown to be clearly better than all others. Thus, the original tissue characterization method developed by Poulin and Theil (Poulin & Theil, 2000) was selected and used to develop an equation for S_t.

$$S_t = S_w \left[K_{vo:w}\left(V_{nt} + 0.3V_{pht}\right) + \left(V_{wt} + 0.7V_{pht}\right) \right], \tag{11}$$

where $S_w$is the solubility of a leachable substance in water, $K_{vo:w}$ is the vegetable oil water partition coefficient, $V_{nt}$is the volume fraction of neutral lipids in tissue, $V_{pht}$is the volume fraction of phospholipids in tissue and $V_{wt}$is the volume fraction of water in tissue.

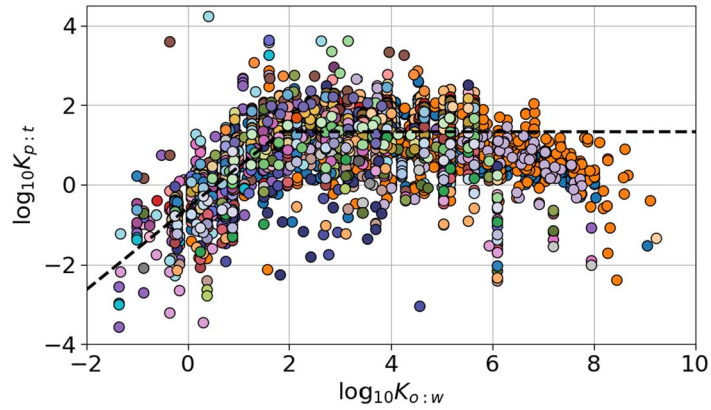

Figure 2 The polymer tissue partition coefficient shows that the data may be clustered into two general groups. Each polymer is shown with a different colour. Solutes with M_w <50 g/mol are excluded.

The linear free energy relation (LSER) for the olive oil–water partition coefficient from Abraham *et al.* (2010) was used to calculate $K_{vo:w}$. Abraham parameters needed to employ the LSER were obtained for the solutes from the UFZ-LSER database (Ulrich *et al.*, 2017). When available in the database, experimentally determined Abraham parameters were used. Otherwise, quantitative structure property relations provided by the UFZ-LSER database as described by Brown and coworkers (Brown *et al.*, 2012; Brown, 2014), were used to predict the parameters. Solutes that were outside the domain of applicability were discarded.

Using equation (9), S_t was calculated using data found in published literature. The partition coefficient was found for 57 chemicals (Poulin & Theil, 2000), the water solubility was found for each of these chemicals on PubChem (NIH, 2022a) and go.drugbank.com (Drugbank.com, 2022) and the volume fractions for nine different tissue types were evaluated (Poulin & Theil, 2000). In total, 513 data points were evaluated. Examination of the results supports the use of a single standard tissue model as a simplified approximation for most tissues (e.g. muscle, liver, lung, kidney, brain, etc.). In this study, muscle tissue with the following properties (Utsey *et al.*, 2020), V_{nt}= 0.013, V_{pht}= 0.0072, V_{wt}= 0.748, were used to represent all tissue in the $K_{p:t}$ calculations (Utsey *et al.*, 2020).

Knowing S_p for a multitude of chemical–polymer combinations and S_t for the tissue standard enables the calculation of $K_{p:t}$ (Fig. 2). Leachable substances that are more hydrophilic seem to have a linear relationship between $\log_{10}K_{p:t}$ and $\log_{10}K_{o:w}$. In contrast, leachable substances that are more hydrophobic seem to have a $\log_{10}K_{p:t}$ value that is independent of $\log_{10}K_{o:w}$. Fitting the data resulted in the relationship,

$$\log_{10}K_{p:t} = \begin{cases} (1.03 \pm 0.03)\log_{10}K_{o:w} - 0.57 \pm 0.03 & \log_{10}K_{o:w} < 1.8 \\ 1.32 \pm 0.01 & \log_{10}K_{o:w} \geq 1.8 \end{cases} \quad (12)$$

where the values after ± are the standard errors of the fitting parameters, calculated as the square root of the diagonal of the covariance matrix. The behaviour may be explained by considering the chemical nature of polymers and tissues. Polymers used in medical devices tend to be highly hydrophobic unless they are specifically designed to be hydrophilic (Schmidt, 2019). The single standard tissue model

Table 3 *$Log_{10}K_{p:t}$ quantiles*

Quantile	5%	25%	Median	75%	95%
Value	−1.11	0.51	1.33	1.75	2.50

consists mostly of water (74.8%), but it also has about 2% hydrophobic lipids. For hydrophilic leachable substances, it seems reasonable that $K_{p:t}$ is proportional to the hydrophilicity because the leachable substance will preferentially dissolve in the mostly water-based tissue. However, for hydrophobic leachable substances that tend to stay within the polymer, there is a limit to how high $K_{p:t}$ can go because the tissue also has hydrophobic lipids, so the maximum ratio is about 50:1.

Data in Fig. 2 were analysed to determine the median polymer–tissue partition coefficient for all polymers in the data set, the upper and lower quartiles and the 5% and 95% values (Table 3). Data that spans the 5% to 95% range from $\log_{10}K_{p:t} = -1.11$to $\log_{10}K_{p:t} = 2.50$. This range was used to establish the input parameter range for $K_{p:t}$.

1.2.3. *Estimating diffusion coefficients within a tissue.* A comprehensive literature review was performed to acquire data to quantify the diffusion coefficients and the solubility of various solutes in biological tissue. A systematic search using SciFinder (ACS, 2022), Medline/PubMed (NIH, 2022b) and Google Scholar (Google, 2023) was conducted using several keywords and phrases. In addition, forward and backward snowballing (Jalali & Wohlin, 2012) were used to identify studies that may have been overlooked in the systematic search. Keywords included "tissue", "diffusion", "diffusion coefficient" and other similar words searched both independently and together. Other keywords included specific tissue types like "brain", "skin", "muscle" and units of diffusion like "cm^2/s" or "$m^2\ s^{-1}$"

The literature search revealed that many of the papers found when searching for tissue diffusion did not contain quantitative values useful in this study. Many papers cited the apparent diffusion coefficient, a measure of water diffusivity in tissue found using magnetic resonance imaging (Herneth *et al.*, 2003; Ren & Lu, 2019; Maynard *et al.*, 2020; Surov *et al.*, 2020). Others focused on the diffusion of oxygen and other gases (Macdougall & Mccabe, 1967; Garrido *et al.*, 2008; Pias, 2020). Some examined plant tissue (Philip, 1958; Kolomazník *et al.*, 2012; Wu & Zhang, 2019). This limited the number of applicable articles. However, several researchers provided quantitative diffusion coefficients for leachable substances in tissue obtained experimentally using a variety of methods. Tissue types included dermatomed skin, the whole epidermis, the stratum corneum, the dermis layer (Ellison *et al.*, 2020), colon carcinoma cells (Pruijn *et al.*, 2008), tumour cell cultures (Hicks *et al.*, 2010), brain cortex in living rats (Meulemans *et al.*, 1989), endovascular and perivascular arterial parenchyma (Creel *et al.*, 2000) and bovine arteries transmural and parallel to the surface (Hwang & Edelman, 2002; Levin *et al.*, 2004; Kolachalama *et al.*, 2013). Measurement methods included ABL diffusion resistance (Ellison *et al.*, 2020), multicellular layer (MCL) flux (Pruijn *et al.*, 2008; Hicks *et al.*, 2010), microelectrodes (Meulemans *et al.*, 1989), liquid scintillation spectroscopy (Creel *et al.*, 2000; Levin *et al.*, 2004; Kolachalama *et al.*, 2013) and fluorescence (Hwang & Edelman, 2002). A summary of these data is shown in Table 4.

From these sources, tissue diffusion values were found for 307 different combinations of chemicals and tissues (see Supplemental Information—Tissue Diffusion Data, SI4). These were grouped into barrier tissues (red) and non-barrier tissues (blue) (Fig. 3) (Tanaka *et al.*, 2023). Barrier tissues were defined as tissues that function to resist the transmission of substances through their surface. Examples include transmural transport through an artery wall and transmission across the stratum corneum or intact

Table 4 *Summary of tissue diffusion sources*

Number of chemicals	Tissue type	Barrier tissue	Temperature (°C)	Method	Author	Year
49	Dermatomed skin (composite)	Yes	22	ABL diffusion resistance	Ellison	2020
50	Whole epidermis (composite)	Yes	22	ABL diffusion resistance	Ellison	2020
49	Stratum corneum	Yes	22	ABL diffusion resistance	Ellison	2020
50	Dermis	No	22	ABL diffusion resistance	Ellison	2020
77	Colon carcinoma cells	No	22	MCL flux	Pruijn	2008
3	Various tumour cell cultures	No	37	MCL flux	Hicks	2010
5	Brain—cortex	No	37	Microelectrodes living rat brain	Meulemans	1989
3	Endovascular arterial parenchyma	Yes	37	Liquid scintillation spectroscopy	Creel	2000
3	Perivascular arterial parenchyma	Yes	37	Liquid scintillation spectroscopy	Creel	2000
5	Artery wall—transmural	Yes	25	Fluorescence in bovine arteries	Hwang	2002
5	Artery wall—parallel	No	25	Fluorescence in bovine arteries	Hwang	2002
3	Artery wall—transmural	Yes	25	Liquid scintillation calf arteries	Levin	2004
3	Artery wall—parallel	No	25	Liquid scintillation calf arteries	Levin	2004
2	Artery wall—transmural	Yes	22	Liquid scintillation porcine arteries	Kolachalama	2022

skin. Examples of non-barrier tissues include brain tissue, tumour cell cultures and arterial transmission parallel to the surface. Curve fitting the tissue diffusion to molecular weight yielded the equation

$$\log_{10} D_t = \begin{cases} (-0.094 \pm 0.126)\ \log_{10} M_w - 7.50 \pm 0.30 & \textit{barrier tissue} \\ (-0.067 \pm 0.112)\ \log_{10} M_w - 6.02 \pm 0.28 & \textit{nonbarrier tissue} \end{cases} \quad (13)$$

Similarly, curve fitting the tissue diffusion to the octanol–water partition coefficient yielded the equation

$$\log_{10} D_t = \begin{cases} (-0.060 \pm 0.045)\ \log_{10} K_{o:w} - 7.62 \pm 0.10 & \textit{barrier tissue} \\ (-0.042 \pm 0.035)\ \log_{10} K_{o:w} - 6.16 \pm 0.06 & \textit{nonbarrier tissue} \end{cases} \quad (14)$$

Table 5 shows the mean value by group and the two inner quartiles (25% and 75%). The 5% and 95% values were estimated from these inner quartiles.

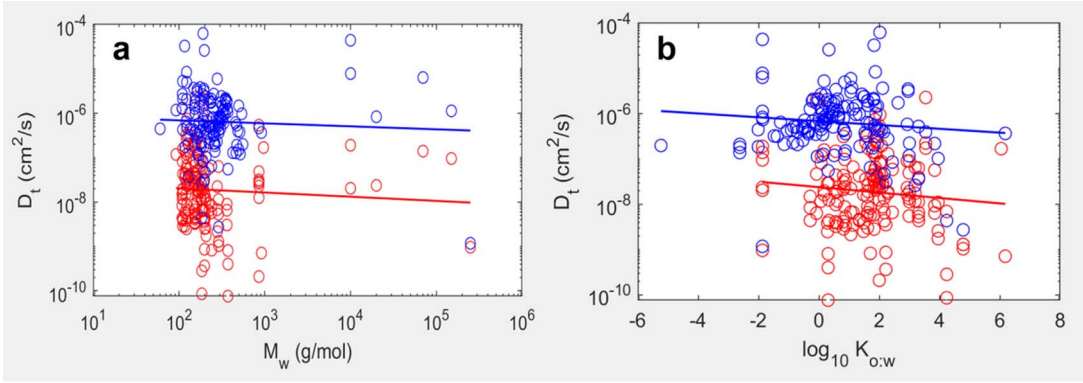

Figure 3 Tissue diffusion data as a function of molecular weight (a) and octanol–water partition coefficient (hydrophobicity) (b).

Table 5 *Diffusion for barrier and non-barrier tissues ($\times 10^{-6}$ cm^2/s)*

Tissue type	5%	25%	Mean	75%	95%
Barrier	0.0010	0.0057	0.020	0.061	0.34
Non-barrier	0.11	0.35	0.65	1.7	5.1

Considering all the different types of leachable substances and the many different tissue types, the 307 data points collected from the literature only represent a small fraction of the possible combinations.

Diffusion through barrier tissue is on the order of 10^{-7} to 10^{-9} cm^2/s. Non-barrier tissue with diffusion coefficients on the order of 10^{-6} to 10^{-7} cm^2/s is about 10 to 100 times higher than barrier tissue. In order to capture the full span of D_t, the range from 5% of barrier tissue to 95% of non-barrier tissue was selected. This equated to an input parameter range for D_t from $10^{-9.0}$ to $10^{-5.3}$ cm^2/s.

1.2.4. *Estimating model input parameter ranges.* Examination of equation (4) shows the quantity of mass released in the two-component model to depend upon both dimensionless parameters, β and τ. The one-component model, equation (7), which does not contain migration limiting elements across the polymer–tissue interface due to the sink boundary condition or diffusion through the surrounding tissue, depends on only one of the dimensionless parameters, τ. Thus, to calculate a suitable range to analyse model behaviour, ranges for β and τ were needed.

Examination of equation (3) shows $\beta$to depend upon the partition coefficient, $K_{p:t}$, and the ratio of the diffusion coefficient through each of the two components in the system (i.e. polymer and tissue). Using the input parameter ranges for $K_{p:t}$, D_t and D_p the analysis range for $\beta$was calculated. The minimum value for β was estimated using equation (3) and applying the highest value within the range of $K_{p:t}$ and D_p, and the lowest value within the range of D_t. Similarly, the maximum value for β was calculated using the other extremes of the input parameter value ranges.

Examination of equation (2) shows $\tau$to depend upon the polymer diffusion coefficient, D_p, and the distance over which diffusion occurs, L (i.e. half the thickness), and time. The time period of the analysis of one day was used based on the current exposure estimation protocols. The diffusion distance, L, was less clearly defined. Recall that the goal of the study is to develop a framework that produces a general

Table 6 *Summary of clinically relevant parameter value ranges*

Parameter	Minimum	Maximum	Range
D_p (cm^2/s)	$10^{-14.7}$	$10^{-4.9}$	$10^{9.8}$
$K_{p:t}$	$10^{-1.1}$	$10^{2.5}$	$10^{3.6}$
D_t (cm^2/s)	$10^{-9.0}$	$10^{-5.3}$	$10^{3.7}$
L (cm)	$10^{-1.3}$	$10^{0.1}$	$10^{1.4}$
β	$10^{-4.6}$	$10^{5.8}$	$10^{10.4}$
τ (at one day)	$10^{-10.0}$	$10^{2.6}$	$10^{12.6}$

solution, and no specific implant was modelled. The thickness of an implanted polymeric product may range from thin films (FILMS, 2023; GlobalSpec, 2023) to thick plates. Thus, a reasonable clinically relevant diffusion distance was defined to be from 0.5 to 12.5 mm.

The model analysis range for the dimensionless parameters, $\beta$and τ, was calculated from the ranges of input parameter values shown in Table 6. The range of $\beta$and τ spanned 14.7 and 15.8 orders of magnitude, respectively.

2. Results

2.1. *Mathematical modelling of daily and monthly mass release*

2.1.1. *Example 1: BPA in silicone.* Consider an implanted medical device made from silicone that is 5 mm thick and has a large enough aspect ratio that it may be considered as a thin sheet (e.g. 50 mm × 50 mm × 5 mm). Assume that BPA is homogeneously distributed throughout the implant with an initial concentration of M_0. Using the modified Piringer equation (8), the molecular weight of BPA = 228 g/mol, and the A_P value for silicone (Table 1: category R1), the diffusion coefficient of the leachable in the polymer, was calculated to be $D_p = 4.7 \times 10^{-7}$ cm^2/s. Equation (12) was used to estimate the value of the the polymer–tissue partition coefficient. Using the octanol–water partition coefficient for BPA ($\log_{10}K_{o:w} \approx 3.5$) from Borrirukwisitsak *et al.* (2012), the polymer–tissue partition coefficient was estimated to be $\log_{10}K_{p:t}$= 1.32. Equation (13) was used to estimate the diffusion coefficient for BPA in silicone. Using the molecular weight of BPA, and assuming a non-barrier tissue, the diffusion coefficient of BPA in tissue was calculated to be $D_t = 6.6 \times 10^{-7}$ cm^2/s. Using equation (14), the octanol–water partition coefficient, and assuming a non-barrier tissue, the diffusion coefficient of BPA in tissue was calculated to be $D_t = 4.9 \times 10^{-7}$ cm^2/s. Averaging these two values results in a value of $D_t = 5.8 \times 10^{-7}$ cm^2/s, which is within 15% of the values obtained using each estimation method.

Given these input parameters, $\log_{10}\beta = -1.27$. Entering these numbers into equation (4) and solving numerically, the mass release for the two-component model was solved as a function of time. The mass release for the one-component model was found by applying these parameters to equation (7) and also solving numerically. Both results are shown in Fig. 4a. For BPA in silicone, the dimensionless time parameter, $\tau = 0.65$, after an evolution time of 24-hour and $\tau = 19.5$ after an evolution time of 30 days. The base 10 log of these dimensionless times are $\log_{10}\tau = -0.187$ and 1.29, respectively. Thus, these cases are examples of highly evolved systems with large values of dimensionless time within the overall range of clinically relevant parameter values (see Table 6).

For BPA in silicone the one-component model estimated complete mass release ($M/M_0 = 100\%$) within about 8 hours, but the more complex two-component model only predicted 35.3% mass release in 24 hours (Fig. 4a). Over a period of 30 days, mass released in the two-component model increased to

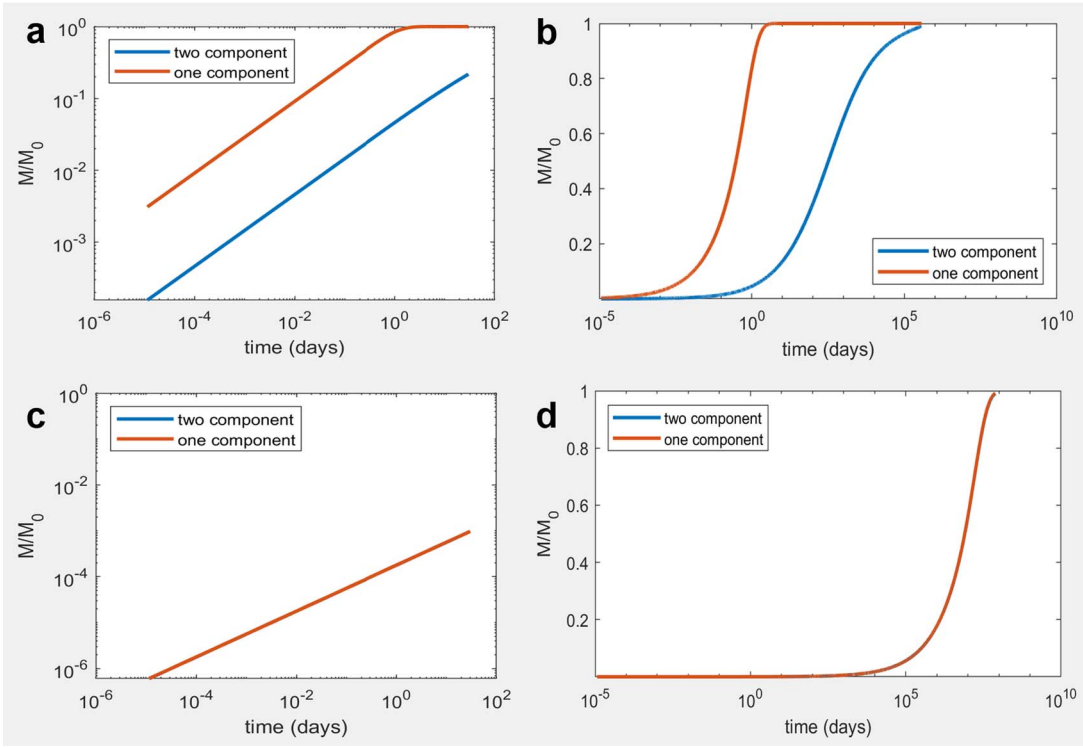

Figure 4 Comparison of model results for cumulative mass release of BPA in silicone (a) and the time required for 99% mass release (b). Irganox 1010 in HDPE evaluated for cumulative mass release (c) and the time required for 99% mass release (d).

78.5%. These findings imply that using the more complex analysis could yield a more clinically relevant outcome in some cases.

2.1.2. *Example 2: Irganox 1010 in HDPE.* Next, consider an implanted medical device made from HDPE that has the same dimensions as the previous example. Assume that Irganox 1010 is homogeneously distributed throughout the implant with an initial concentration of M_0. Using equation (8), the molecular weight of Irganox 1010 = 1178 g/mol, and the A_P value for HDPE (Table 1: category P3), the estimated diffusion coefficient, was calculated to be $D_p = 1.8 \times 10^{-14}$ cm^2/s. Equation (12) was used to estimate the value of the polymer–tissue partition coefficient. Using the octanol–water partition coefficient for Irganox 1010 ($\log_{10}K_{o:w} \approx 19.4$) from PubChem (NIH, 2022a), and assuming a non-barrier tissue, the polymer–tissue partition coefficient was estimated to be $\log_{10}K_{p:t} = 1.32$. Equation (13) was used to estimate the diffusion coefficient for Irganox in HDPE. Using the molecular weight of Irganox 1010, and assuming a non-barrier tissue, the diffusion coefficient of Irganox 1010 in tissue was calculated to be $D_t = 5.9 \times 10^{-7}$ cm^2/s. When approximating D_t using $\log_{10}K_{o:w}$, the value of 19.4 was outside the range of data used to generate the fitted line (Fig. 3b), so the upper limit of the data ($\log_{10}K_{o:w} \approx 6.0$) was used. Using equation (14), the octanol–water partition coefficient, and assuming a non-barrier tissue, the diffusion coefficient of Irganox 1010 in tissue was calculated to be $D_t = 3.9 \times 10^{-7}$ cm^2/s. Averaging these two values results in a value of $D_t = 4.9 \times 10^{-7}$ cm^2/s, which is within 21% of the values obtained using each estimation method.

Given these input parameters, $\log_{10}\beta = 2.40$. The mass release estimated for the one- and two-component models were solved numerically and plotted (Fig. 4c). For these model parameters, the dimensionless time parameter $\tau = 2.49 \times 10^{-8}$ after an evolution time of 24-hour and $\tau = 7.46 \times 10^{-7}$after an evolution time of 30 days. The base 10 logs of these dimensionless times are $\log_{10}\tau = -7.60$ and -6.13, respectively. In this case, the system is evolving very slowly as indicated by the tiny values of dimensionless time.

For Irganox 1010 in HDPE the one-component model and two-component model have virtually identical results with the first line being totally covered by the second. Both models predict a mass release of 0.15% of the total mass in the first 24 hours. Over a period of 30 days, both models estimate a mass release of 0.8%. In this case it may not be beneficial to apply the more complex model when the simpler model predicts the same outcome. The reason for this similarity is that the low polymer diffusion coefficient of Irganox 1010 in HDPE dominates the model behaviour, causing the two-component model to approximate the sink boundary condition used in the one-component model.

2.2. *Mathematical modelling of 99% mass release*

The time required to release 99% of the total mass was determined using both models. For BPA in silicone (Fig. 4b), the one-component model predicts 99% mass release in 4.9 hours (0.20 days) while the two-component model predicts 99% mass release in 43.6 years (15,900 days). Clearly, in this case including the surrounding tissue in the model effected the time required for mass release. For Irganox 1010 in HDPE (Fig. 4d), the one- and two-component model predict 99% mass release in 2940 and 3060 years, respectively. Like in the previous set of images, no visible difference is observable between modelling results for Irganox 1010 in HDPE. While the time required for 99% mass release is not identical, the magnitude of the difference is small when compared to the difference in results when compared to BPA in silicone.

2.3. *Evaluation of models over the range of input parameters*

In the above sections the quantity of mass released was calculated for two specific cases of input parameter values. In this section the solution results will be expanded over the entire analysis range of $\beta$and τ. Mass release is calculated for 1 day of exposure. Because this is a single scalar value for each combination of $\beta$and τ, the results can be plotted as a heat map (Fig. 5a). Examination of the data shows the lowest mass is released when the values of $\beta$and τ are the lowest. When both $\beta$and τ are large, M/M_0 approaches one, indicating complete mass release. This can be seen on the upper right side of the heat map. The one-component model is only controlled by one of the dimensionless parameters, τ. The plot shows that when the value of tau is low, a very small percentage of the mass is released over a 24-hour period (Fig. 5b). As the value of τ approaches one, M/M_0 also approaches one, indicating complete mass release.

The CGR over the input parameter range for β and τ is shown in Fig. 6. Results found using the one-component model were similar to those found with the two-component model (i.e. CGR$\approx$ 1) at higher levels of β. The CGR became larger as β became smaller. It reached a maximum value of $\sim$4000 ($10^{3.6}$) when β was smallest. The magnitude of τ also influenced the CGR. When τ was small ($<10^{-1}$), the magnitude of τ had no noticeable effect on the CGR and contour lines were observed to be generally horizontal. However, for $\tau > 1$, increasing τ caused the CGR to become smaller. Furthermore, when the governing equations are examined, the two-component model (Eq. 4) is identical to the one-component model (Eq. 5) as β approaches infinity (see Supplemental Information—Mathematical Proof, SI). In addition, both equations converge on $M/M_0 = 1$as $\tau \to \infty$. This implies that for both models, as the

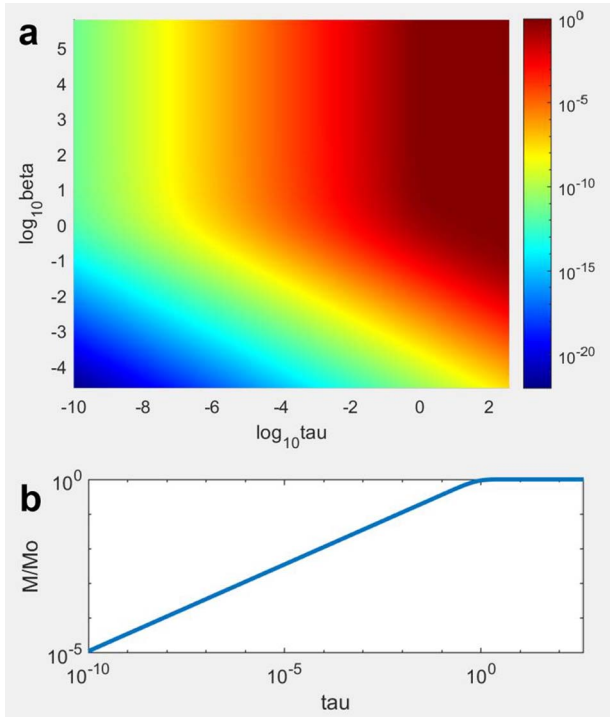

Figure 5 Mathematical model solutions over the range of input parameter values. Mass release for the two-component model is shown as a 2D heat map (a) and for the one-component model as a log–log plot.

dimensionless time approaches infinity, all the mass of a leachable that was within the implanted medical device will be released. This is because the one-component model has a sink boundary condition at the implant–tissue interface and the tissue in the two-component model is infinite.

3. Discussion

The more complex two-component model always predicts a lower quantity of material released than the more conservative one-component model over the same time period. While the one-component model may be more appropriate to support routine estimation of toxicological risk because it is more conservative, differences in predictions could imply that the two-component model could be adopted for some combinations of input parameters depending on the purpose of the model. Examining the results over the input parameter ranges for $K_{p:t}$, D_t and D_p revealed that conditions exist where little difference in results is observed between the one- and two-component models (i.e. CGR$\approx$ 1). In these cases, it is better to use the simpler one-component model. Examination of Fig. 6 shows that the transition to CGR$\approx$ 1 occurs somewhere around β values of 10^0 and 10^1 for smaller values of τ. These findings are consistent with Gandek who used a value of $\beta > 10$ to decide if the polymer food surface should be considered well mixed or migration should be controlled by diffusive transport (Gandek, 1986).

When the value of β is low, using the two-component model could dramatically impact the estimated value of material released. In this study, a mass release$\sim$40,000 times lower was predicted for the most

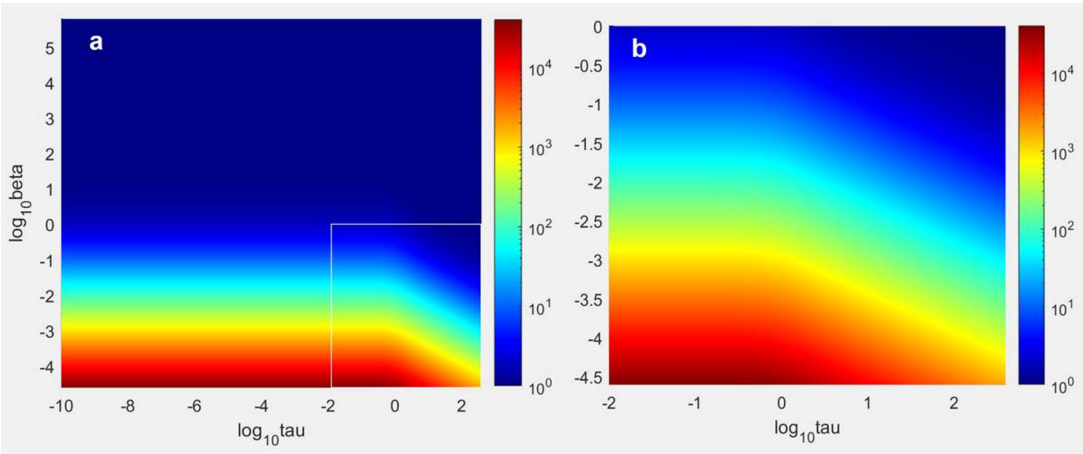

Figure 6 CGR over the typical range of input parameter values. The CGR is shown for the (a) the entire range and (b) for a close-up section.

extreme case, which equates to 4.6 orders of magnitude. Moreover, for about 20% of the evaluated conditions, the one-component model predicts a mass release at least 100× greater than the two-component model. Thus, if used as a mechanism to estimate mass release either at the early stages of product design or as part of a regulatory submission, selecting the appropriate model may make the difference between passing and failing to meet tolerable limits. It is important to note that the actual amount of material released by a polymeric device does not change, only the complexity and level of conservatism of the approximation.

Thus, it is important to determine which conditions lead to small values of β. Examining equation (3) it is clear that β depends upon two factors. The first factor is the polymer tissue partition coefficient, $K_{p:t}$. Because of the inverse relationship, β becomes smaller as $K_{p:t}$ increases. By definition, higher values of $K_{p:t}$exist when a leachable substance is more soluble in the polymer than the tissue. Leachables that satisfy this requirement tend to be hydrophobic, having higher solubility in the typically hydrophobic polymer than the generally aqueous tissue. This concept is supported by the results shown in Fig. 2 where higher values of $K_{p:t}$ are observed when the octanol water partition coefficient $K_{o:w}$ is high. However, the presence of hydrophobic lipids in the tissue will always allow some hydrophobic leachables to be dissolved, limiting how high $K_{p:t}$ can become. In the mathematical model, values of $K_{p:t}$ >1 reduce the concentration gradient within the polymer and slows diffusive transport of leachables from the interior of the implant to its surface. The second factor is the ratio of D_t to D_p. In other words, it is a measure of the relative rate that a leachable travels through the second component (tissue) to the first (polymer). Beta is low when the leachable travels more quickly through the polymer than the tissue. If D_p exceeds D_t, leachables can travel to the surface faster than they can be removed, which, like the influence of $K_{p:t}$, has the effect of reducing diffusive transport away from the polymer.

Another potential use for these models is to put bounds on mass release estimates. Because the one-component model tends to be conservative and overestimates mass release it is a good candidate to use for the upper bound. It eliminates the need to estimate a partition coefficient or tissue diffusion coefficient by using a sink boundary condition at the implant surface. Thus, there is no resistance to migration

in this model beyond Fickian diffusion of the leachable through the polymer. The two-component model takes into account more system parameters in the mass release estimation including the polymer–tissue partition coefficient and diffusion through the tissue. These factors can influence the migration of leachables, reducing the rate of release. Because the two-component model always predicts a lower migration rate, it may be used as a lower bound estimation. While the upper bound is well defined based on known polymer properties and leachable characteristics, the lower bound is not as clear. Its ability to predict migration of leachables depends on the validity of the model assumptions and the behaviour of complex heterogeneous biological systems. Using a quasistatic homogeneous tissue model to predict leaching over longer periods should only be considered an initial approximation. This enabled the use of time-independent parameter values for $K_{p:t}$, D_p and D_t, which simplified the modelling. However, additional adaptations may be required to apply this model to capture changes in tissue properties that may occur over time. It is well known that implanted foreign bodies can cause histomorphological changes in tissue near the implant surface resulting in encapsulation (Sharkawy *et al.*, 1998; Novak *et al.*, 2010; Damanik *et al.*, 2014; Klopfleisch & Jung, 2017). These changes would cause D_t and $K_{p:t}$ to change as well. Thus, further investigation is needed to consider how changes in tissue properties over time could impact the results. However, even with these limitations, the current models can reveal trends in behaviour that may be present in more complex models.

Currently there is a lack of clinical data to validate these models. Data used for the model input parameters were collected from a multitude of studies, each of which measured these parameters for a different purpose. No experiments were conducted as part of this study to explicitly collect data for use in the models. Fortunately, diffusion coefficients of leachables within polymers tended to be types that are released from a medical device such as additives, contaminants and unprocessed oligomers. Because of this, the diffusion coefficient within device-relevant polymers is well characterized (Elder & Saylor, 2023). However, studies designed to measure diffusion through tissue tended to measure the diffusion coefficient of drugs rather than medical device relevant leachables. Thus, there is less relevant data available to characterize the diffusion coefficient in tissue. Experimental data used to calculate the ranges for $K_{p:t}$, D_p and D_t are sparse, only representing a small fraction of the possible number of combinations. However, even with these limitations, they were observed to span an adequate range of molecular weight and hydrophobicity. Future experiments that measure all the input parameters, $K_{p:t}$, D_p and D_t, for a specific leachable substance, in a specific polymer type, and diffusing through a specific type of tissue would provide excellent data for model validation. Yet, even with the limitations and lack of data for validation, the models provide an initial approximation to characterize the complex fate of leachables contained within implanted medical devices and the influence of the polymer–tissue interface and the tissue surrounding the implant.

4. Conclusion

Two mathematical models were used to characterize the mass release from a polymeric implant, a more complex two-component model, and a simpler one-component model. The models included two dimensionless parameters, β and τ, that controlled the results. When β was large, there was minimal difference in the quantity of mass release estimated using either model, so in this case it would be better to use the simpler one. However, when β was small, the difference in the model prediction could be quite high, on the level of three orders of magnitude. In this case, use of the more complex model may be warranted. While it is difficult to say if one model is better than the other, the two models can be used together as an upper bound estimation (one-component model) and a lower bound estimation (two-component model) for leaching of substances from an implanted polymeric medical device.

Acknowledgements

This research was supported by a grant from the National Science Foundation, USA—Award #2149517 and #2309538. The authors express appreciation to William J. Tanaka for his assistance with the mathematical proof in the supplemental information.

DISCLAIMER

The findings and conclusions in this manuscript have not been formally disseminated by the FDA and should not be construed to represent any agency determination or policy. The mention of commercial products, their sources or their use in connection with material reported herein is not to be construed as either an actual or implied endorsement of such products by the Department of Health and Human Services.

References

Abraham, M. H., Smith, R. E., Luchtefeld, R., Boorem, A. J., Luo, R., Acree, J. R. & W. E. (2010) Prediction of solubility of drugs and other compounds in organic solvents. *J Pharm Sci*, **99**, 1500–1515.

ACS. (2022) *SciFinder—American Chemical Society* [Online]. Available: https://scifinder.cas.org/ (26 August 2022, Date accessed).

Berezhkovskiy, L. M. (2004) Volume of distribution at steady state for a linear pharmacokinetic system with peripheral elimination. *J Pharm Sci*, **93**, 1628–1640.

Borrirukwisitsak, S., Keenan, H. E. & Gauchotte-Lindsay, C. (2012) Effects of salinity, pH and temperature on the octanol-water partition coefficient of bisphenol A. *Int J Environ Sci Dev*, **3**, 460.

Brown, T. N. (2014) Predicting hexadecane–air equilibrium partition coefficients (L) using a group contribution approach constructed from high quality data. *SAR QSAR Environ Res*, **25**, 51–71.

Brown, T. N., Arnot, J. A. & Wania, F. (2012) Iterative fragment selection: A group contribution approach to predicting fish biotransformation half-lives. *Environ Sci Technol*, **46**, 8253–8260.

Chandrasekar, V., Janes, D. W., Forrey, C., Saylor, D. M., Bajaj, A., Duncan, T. V., Zheng, J., Riaz Ahmed, K. B. & Casey, B. J. (2018) Improving risk assessment of color additives in medical device polymers. *J Biomed Mater Res B Appl Biomater*, **106**, 310–319.

Crank, J. (1975) *The Mathematics of Diffusion*, 2nd edn. Oxford: Claredon Press.

Creel, C. J., Lovich, M. A. & Edelman, E. R. (2000) Arterial paclitaxel distribution and deposition. *Circ Res*, **86**, 879–884.

Damanik, F. F., Rothuizen, T. C., Van Blitterswijk, C., Rotmans, J. I. & Moroni, L. (2014) Towards an in vitro model mimicking the foreign body response: Tailoring the surface properties of biomaterials to modulate extracellular matrix. *Sci Rep*, **4**, 1–11.

Dortmund. (2023) *DDBST Dortmund Data Bank Software &. Separation Technology GmbH* [online]. Available: https://www.ddbst.com/ (29 August 2022, Date accessed).

DRUGBANK.COM. (2022) *Drugbank Online* [Online]. Available: https://go.drugbank.com/ (26 August 2022, Date accessed).

Elder, R. M. & Saylor, D. M. (2023) Robust estimates of solute diffusivity in polymers for predicting patient exposure to medical device leachables. *J Polym Sci*, **61**, 2163–2180.

Ellison, C. A., Tankersley, K. O., Obringer, C. M., Carr, G. J., Manwaring, J., Rothe, H., Duplan, H., Géniès, C., Grégoire, S. & Hewitt, N. J. (2020) Partition coefficient and diffusion coefficient determinations of 50 compounds in human intact skin, isolated skin layers and isolated stratum corneum lipids. *Toxicol In Vitro*, **69**, 104990.

FDA. (2023) *Use of International Standard ISO 10993-1, "Biological evaluation of medical devices—Part 1: Evaluation and testing within a risk management process"* [Online]. Available: https://www.fda.gov/regulatory-information/search-fda-guidance-documents/use-international-standard-iso-10993-1-biological-evaluation-medical-devices-part-1-evaluation-and (13 October 2023, Date accessed).

FILMS, S.-G. P. P.-S. (2023) *CHEMFILM® FEP Fluoropolymer Film* [Online]. Available: https://pdf.aeroexpo.online/pdf/saint-gobain-performance-plastics-specialty-films/chemfilm-fep-fluoropolymer-film/170459-5878.html (14 June 2023, Date accessed).

Gandek, T. P. (1986) *Migration of Phenolic Antioxidants from Polyolefins to Aqueous Media with Application to Indirect Food Additive Migration.* Ph.D. Thesis, Massachusetts Institute of Technology, Cambridge, MA, USA.

Garrido, L., López-González, M., Saiz, E. & Riande, E. (2008) Molecular basis of carbon dioxide transport in polycarbonate membranes. *J Phys Chem B*, **112**, 4253–4260.

GLOBALSPEC. (2023) *MEDICAL / FOOD (FDA, USDA) PLASTIC SHEET AND PLASTIC FILM* [Online]. Available: https://www.globalspec.com/ds/4397/areaspec/industry_medical (14 July, Date accessed).

GOOGLE. (2023) *Google Scholar* [Online]. Available: https://scholar.google.com/ (26 August 2022, Date accessed).

Haddadin, R., Qian, F., Desikan, S., Hussain, M. & Smith, R. L. (2009) Estimation of drug solubility in polymers via differential scanning calorimetry and utilization of the fox equation. *Pharm Dev Technol*, **14**, 19–27.

Herneth, A. M., Guccione, S. & Bednarski, M. (2003) Apparent diffusion coefficient: A quantitative parameter for in vivo tumor characterization. *Eur J Radiol*, **45**, 208–213.

Hicks, K. O., Siim, B. G., Jaiswal, J. K., Pruijn, F. B., Fraser, A. M., Patel, R., Hogg, A., Liyanage, H., Dorie, M. J., Brown, J. M., Denny, W. A., Hay, M. P. & Wilson, W. R. (2010) Pharmacokinetic/pharmacodynamic modeling identifies SN30000 and SN29751 as tirapazamine analogues with improved tissue penetration and hypoxic cell killing in Tumors. Hypoxic cytotoxicity of improved tirapazamine analogues. *Clin Cancer Res*, **16**, 4946–4957.

Hwang, C.-W. & Edelman, E. R. (2002) Arterial ultrastructure influences transport of locally delivered drugs. *Circ Res*, **90**, 826–832.

Jalali, S. & Wohlin, C. (2012) *Systematic Literature Studies: Database Searches vs. Backward Snowballing*. Proceedings of the 2012 ACM-IEEE International Symposium on Empirical Software Engineering and Measurement, Lund Sweden, 20–21 Sept. 2012. New York, NY, USA: Association for Computing Machinery, pp. 29–38.

Klopfleisch, R. & Jung, F. (2017) The pathology of the foreign body reaction against biomaterials. *J Biomed Mater Res A*, **105**, 927–940.

Kolachalama, V. B., Pacetti, S. D., Franses, J. W., Stankus, J. J., Zhao, H. Q., Shazly, T., Nikanorov, A., Schwartz, L. B., Tzafriri, A. R. & Edelman, E. R. (2013) Mechanisms of tissue uptake and retention in zotarolimus-coated balloon therapy. *Circulation*, **127**, 2047–2055.

Kolomazník, K., Pecha, J., Friebrová, V., Janáčová, D. & Vašek, V. (2012) Diffusion of biostimulators into plant tissues. *Heat Mass Transf*, **48**, 1505–1512.

Levin, A. D., Vukmirovic, N., Hwang, C.-W. & Edelman, E. R. (2004) Specific binding to intracellular proteins determines arterial transport properties for rapamycin and paclitaxel. *Proc Natl Acad Sci*, **101**, 9463–9467.

Lippert, J., Burghaus, R., Edginton, A., Frechen, S., Karlsson, M., Kovar, A., Lehr, T., Milligan, P., Nock, V., Ramusovic, S., Riggs, M., Schaller, S., Schlender, J., Schmidt, S., Sevestre, M., Sjögren, E., Solodenko, J., Staab, A. & Teutonico, D. (2019) Open systems pharmacology community—an open access, open source, open science approach to modeling and simulation in pharmaceutical sciences. *CPT Pharmacometrics Syst Pharmacol*, **8**, 878–882.

Macdougall, J. D. B. & Mccabe, M. (1967) Diffusion coefficient of oxygen through tissues. *Nature*, **215**, 1173–1174.

Mańin, A. P., Tatarenko, L. A. & Shlyapnikov, Y. A. (1998) Solubility of antioxidants in poly(vinyl butyral). *Polym Degrad Stab*, **62**, 507–511.

Maynard, J., Okuchi, S., Wastling, S., Busaidi, A. A., Almossawi, O., Mbatha, W., Brandner, S., Jaunmuktane, Z., Koc, A. M., Mancini, L., Jäger, R. & Thust, S. (2020) World Health Organization grade II/III glioma molecular status: Prediction by MRI morphologic features and apparent diffusion coefficient. *Radiology*, **296**, 111–121.

Meulemans, A., Paycha, F., Hannoun, P. & Vulpillat, M. (1989) Measurement and clinical and pharmacokinetic implications of diffusion coefficients of antibiotics in tissues. *Antimicrob Agents Chemother*, **33**, 1286–1290.

NIH. (2022a) *PubChem* [Online]. Available: https://pubchem.ncbi.nlm.nih.gov/ (26 August 2022, Date accessed).

NIH. (2022b) *PubMed* [Online]. Available: https://pubmed.ncbi.nlm.nih.gov/ (29 August 2022, Date accessed).

Novak, M. T., Yuan, F. & Reichert, W. M. (2010) Modeling the relative impact of capsular tissue effects on implanted glucose sensor time lag and signal attenuation. *Anal Bioanal Chem*, **398**, 1695–1705.

Philip, J. R. (1958) Osmosis and diffusion in tissue: Half-times and internal gradients. *Plant Physiol*, **33**, 275–278.

Pias, S. C. (2020) Pathways of oxygen diffusion in cells and tissues : Hydrophobic channeling via networked lipids. *Adv Exp Med Biol*, **1232**, 183–190.

Piringer, O. G. & Baner, A. L. (2008) *Plastic Packaging: Interactions with Food and Pharmaceuticals*. Hoboken, NJ, USA: John Wiley & Sons.

Poulin, P. & Theil, F. P. (2000) A priori prediction of tissue: Plasma partition coefficients of drugs to facilitate the use of physiologically-based pharmacokinetic models in drug discovery. *J Pharm Sci*, **89**, 16–35.

Poulin, P. & Theil, F. P. (2002) Prediction of pharmacokinetics prior to in vivo studies. 1. Mechanism-based prediction of volume of distribution. *J Pharm Sci*, **91**, 129–156.

Poulin, P., Schoenlein, K. & Theil, F. P. (2001) Prediction of adipose tissue: Plasma partition coefficients for structurally unrelated drugs. *J Pharm Sci*, **90**, 436–447.

Pruijn, F. B., Patel, K., Hay, M. P., Wilson, W. R. & Hicks, K. O. (2008) Prediction of tumour tissue diffusion coefficients of hypoxia-activated prodrugs from physicochemical parameters. *Aust J Chem*, **61**, 687–693.

Ren, H. & Lu, H. (2019) Dynamic features of brain edema in rat models of traumatic brain injury. *Neuroreport*, **30**, 605–611.

Rodgers, T. & Rowland, M. (2006) Physiologically based pharmacokinetic modelling 2: Predicting the tissue distribution of acids, very weak bases, neutrals and zwitterions. *J Pharm Sci*, **95**, 1238–1257.

Rodgers, T., Leahy, D. & Rowland, M. (2005) Physiologically based pharmacokinetic modeling 1: Predicting the tissue distribution of moderate-to-strong bases. *J Pharm Sci*, **94**, 1259–1276.

Saylor, D. M., Chandrasekar, V., Simon, D. D., Turner, P., Markley, L. C. & Hood, A. M. (2019) Strategies for rapid risk assessment of color additives used in medical devices. *Toxicol Sci*, **172**, 201–212.

Saylor, D. M., Chandrasekar, V., Elder, R. M. & Hood, A. M. (2020) Advances in predicting patient exposure to medical device leachables. *Med Devices Sens*, **3**, e10063.

Schmidt, B. V. K. J. (2019) Hydrophilic polymers. *Polymers*, **11**, 693.

Schmitt, W. (2008) General approach for the calculation of tissue to plasma partition coefficients. *Toxicol In Vitro*, **22**, 457–467.

Schwope, A. D., Goydan, R, & Reid, R C. (1992) *Methods for Assessing Exposure to Chemical Substances*. Volume **11**. Methodology for Estimating the Migration of Additives and Impurities from Polymeric Materials. U.S. Environmental Protection Agency, Washington, DC.

Sharkawy, A. A., Klitzman, B., Truskey, G. A. & Reichert, W. M. (1998) Engineering the tissue which encapsulates subcutaneous implants. III. Effective tissue response times. *J Biomed Mater Res*, **40**, 598–605.

Suné, N. M. (2006) *Prediction of Solubility and Diffusion Properties of Pesticides in Polymers.* Ph.D. thesis, Technical University of Denmark, Kongens Lyngby, Denmark

Surov, A., Meyer, H. J. & Wienke, A. (2020) Correlations between apparent diffusion coefficient and Gleason score in prostate cancer: A systematic review. *Eur Urol Oncol*, **3**, 489–497.

Tanaka, M., Saylor, D. & Elder, R. (2023) Tissue diffusion and two component computational model to predict leaching from medical devices. *Summer Biomechanics, Bioengineering and Biotransport Conference*. Vail, CO, USA: Sb3C Foundation Inc, Fairfield, CT, USA.

Turner, P., Elder, R. M., Nahan, K., Talley, A., Shah, S., Duncan, T. V., Sussman, E. M. & Saylor, D. M. (2020) Leveraging extraction testing to predict patient exposure to polymeric medical device Leachables using physics-based models. *Toxicol Sci*, **178**, 201–211.

Ulrich, N., Endo, S., Brown, T. N., Watanabe, N., Bronner, G., Abraham, M. H. & Goss, K.-U. (2017) *LSER Database v 3.2.1 [Online]*. Helmholtz Centre for Environmental Research-UFZ, Leipzig, Germany. Available: http://www.ufz.de/lserd Accessed 4 June 2022.

Utsey, K., Gastonguay, M. S., Russell, S., Freling, R., Riggs, M. M. & Elmokadem, A. (2020) Quantification of the impact of partition coefficient prediction methods on physiologically based pharmacokinetic model output using a standardized tissue composition. *Drug Metab Dispos*, **48**, 903–916.

Willmann, S., Lippert, J. & Schmitt, W. (2005) From physicochemistry to absorption and distribution: Predictive mechanistic modelling and computational tools. *Expert Opin Drug Metab Toxicol*, **1**, 159–168.

Wu, Y. & Zhang, D. (2019) Pulsed electric field enhanced freeze-drying of apple tissue. *Czech J Food Sci*, **37**, 432–438.